Analytical solutions for excess pore water pressures generated by TBM tunnelling in a semi-confined aquifer

Xu, Tao; Bezuijen, Adam; Broere, Wout

DOI
10.1016/j.tust.2021.104162

Publication date
2021

Document Version
Final published version

Published in
Tunnelling and Underground Space Technology

Citation (APA)
Xu, T., Bezuijen, A., & Broere, W. (2021). Analytical solutions for excess pore water pressures generated by TBM tunnelling in a semi-confined aquifer. *Tunnelling and Underground Space Technology*, *118*, Article 104162. https://doi.org/10.1016/j.tust.2021.104162

Tunnelling and Underground Space Technology 118 (2021) 104162

Contents lists available at ScienceDirect

Tunnelling and Underground Space Technology incorporating Trenchless Technology Research

journal homepage: www.elsevier.com/locate/tust

Analytical solutions for excess pore water pressures generated by TBM tunnelling in a semi-confined aquifer

Tao Xu [a,*], Adam Bezuijen [b], Wout Broere [c]

[a] Southeast University, School of Transportation, Nanjing, China
[b] Ghent University, Laboratory of Geotechnics, Ghent, Belgium & Deltares, Geo-Engineering, Delft, the Netherlands
[c] Delft University of Technology, Geo-Engineering, Delft, the Netherlands

ARTICLE INFO

Keywords:
Analytical solution
Excess pore water pressure
TBM Tunnelling
Semi-confined aquifer
Slurry infiltration

ABSTRACT

Tunnel-boring machine (TBM) tunnelling through an aquifer will generate excess pore water pressures in the soil around the tunnel face. Accurately predicting the magnitude of the excess pore water pressures is significant because it directly determines the effective face support pressure. In this study, an analytical solution for transient cylindrical flow caused by TBM tunnelling considering the elastic storage of the aquifer is developed. Furthermore, a quasi-static solution to couple the effect of slurry infiltration with the elastic storage is presented. It is shown that the pore water pressures derived from the analytical solution match quite well with the measurements obtained in proximity to as well as far away from the TBM. The coupled quasi-static solution also agrees with the measurements for the places close to the tunnel face, but underestimates the observations far away from the tunnel face. The results also show that a larger infiltration distance leads to a slower dissipation of excess pore water pressures, which does not make a difference during excavation (when excavation velocity is faster than the pore fluid velocity).

1. Introduction

During tunnel-boring machine (TBM) tunnelling with active face support using slurry in an aquifer, the tunnelling can be influenced by soil permeability, soil layering, slurry pressure and tail void grouting etc. Around the tunnel face, excess pore water pressures can be generated by slurry infiltration (Broere, 2001, 2002, Bezuijen, 2002, Hoefsloot, 2001, Bezuijen et al., 2016, Zizka et al., 2017). Other geotechnical factors, such as grouting, may also generate excess pore water pressures (Wang et al., 2020; Wu et al., 2020a, 2020b). Excess pore water pressures generated by TBM tunnelling have been observed at several tunnel projects in the Netherlands, such as the Second Heinenoord Tunnel, the Botlek Rail Tunnel, the Green Hart Tunnel (GHT) and the tunnel of the Amsterdam North/South Metro Line (N/S Line) (Broere, 2001, 2003, Bezuijen, 2002, Bezuijen et al., 2001, 2016, Kaalberg et al., 2014), in China, such as the Middle Ring Tunnel across Huangpu River in Shanghai (Zheng et al., 2006) and in USA, such as the Alaskan Way Viaduct replacement tunnel in the city of Seattle (Cording, 2018). All these tunnels were bored through aquifers. In the case of tunnelling through a semi-confined aquifer, for example a sand layer overlain by a peat or clay layer, the area over which excess pore water pressures will be present is larger than in an unconfined aquifer. Apart from the unfavorable influence on the effective face support, there is in a semi-confined aquifer a risk that the excess pore water pressure may induce cracks in the less permeable upper layer, creating a communication between the aquifer and the free water table or in extreme cases even lifting of the less permeable layers. As a result, for example, brackish water coming from the artesian water table can pollute the agricultural lands (Autouri and Minec, 2005). This situation is also commonly encountered in the delta areas in America, Africa and China (Bohlke et al., 1996; Hamza et al., 1999; Min et al., 2015). Identifying the mechanisms and the magnitude of the excess pore water pressures caused by TBM tunnelling is of significance for the safety of tunnelling and long term economy of agriculture in these areas.

Within a certain project, it is possible to perform a detailed numerical simulation to calculate the excess pore water pressures to be expected around the TBM, see for example Autuori and Minec (2005) and Kaalberg et al. (2014). However, analytical solutions or simple numerical solutions are useful, for a general understanding of the conditions significant where excess pore water pressures can be expected and to study which parameters are of primary importance. Moreover, these are relatively straightforward to include in the current models of tunnel face

* Corresponding author.
E-mail address: taoxu@seu.edu.cn (T. Xu).

https://doi.org/10.1016/j.tust.2021.104162
Received 21 April 2020; Received in revised form 21 January 2021; Accepted 24 August 2021
Available online 13 September 2021

stability. Bezuijen (2002) proposed a radial steady state model for the excess pore water pressure caused by TBM tunnelling in an unconfined aquifer where the soil is homogeneous. Zizka et al. (2017) show that the pore water pressure distribution in front of the TBM, estimated by this model results in an excellent match with the results measured on the axis of the tunnel in front of the TBM. This model was extended to a non-steady state model (Bezuijen et al., 2016) that can calculate the pore water pressure variations by considering the properties of the slurry that infiltrates into the soil. Broere (2001) employed a transient one-dimensional (1-D) linear flow model to predict the excess pore water pressures caused by TBM tunnelling in a semi-confined aquifer. The non-steadiness of the groundwater flow is governed by the elastic storage of the aquifer.

In fact, the groundwater flow caused by TBM tunnelling is more complicated than a 1-D flow. One finding from the observations at the GHT was that there were still some excess pore water pressures even 100 m far away from the TBM perpendicular to the tunnel axis (Xu and Bezuijen, 2018). This means that the flow caused by the TBM tunnelling is not a 1-D flow, but is a complex three-dimensional (3-D) flow problem, that can be approximated by a combination of spherical flow and cylindrical flow around a vertical axis (Bezuijen and Xu, 2018), as will be detailed later. Therefore, a cylindrical flow model will be employed to describe the excess pore water pressures caused by TBM tunnelling in the semi-confined aquifer. Because the semi-confined aquifer has an influence, the formula for homogeneous soil proposed by Bezuijen (2002) cannot be used for this situation. It is also realised that the transient models in Broere (2002) and Xu and Bezuijen (2018) are not exact, because these models assume a constant discharge at the tunnel face instead of a constant piezometric head, as will occur, e.g. at the GHT. However, as an analytical solution for 3-D groundwater flow given these boundary conditions has not been found, a numerical solution assuming a constant discharge will be used.

In this study, first a numerical model for groundwater flow in a semi-confined aquifer is developed, based on a boundary condition of constant piezometric head at the tunnel face. The applicability of this model will be verified with the measurements from the GHT. Furthermore, the difference between the linear flow solution proposed by Broere (2001) and the cylindrical solution will be discussed, and their limitations will be shown. Broere (2002) suggests that slurry infiltration at the tunnel face occurs in a very short period and that the increase or decrease in pore pressure when excavation starts or stops is influenced by elastic storage. Therefore, it is of interest to consider the excess pore water pressure if plastering plays a role. The model considering the effect of slurry infiltration needs be coupled with the cylindrical symmetric solution considering the elastic storage of the semi-confined aquifer. This will allow determining which of these parameters dominates the observed pressure increases and decreases at GHT.

2. Models

2.1. Cylindrical symmetric solution

Some distance away from the TBM (more than the height of the aquifer), the groundwater flow caused by TBM tunnelling in a semi-confined aquifer is deemed almost identical to a cylindrical flow caused by a discharging well in a semi-confined aquifer, and hence the model proposed by Jacob (1946) is employed in this study. The boundary conditions of the aquifer where the TBM is located are shown in Fig. 1. A permeable (sand) layer resting on an impermeable base is overlain by a semi-permeable (peat or clay) layer. The TBM is completely located in the permeable layer. For a semi-confined aquifer, there will be upward leakage through the semi-pervious layer and the groundwater flow in the aquifer is assumed to be horizontal cylindrical flow throughout the aquifer, because the leakage length will in most cases be much larger than the thickness of the aquifer. The cylindrical flow decreases in magnitude as a function of the distance from the tunnel face. It is also assumed that the volume of water released from elastic storage at each location within the aquifer is proportional to the decline

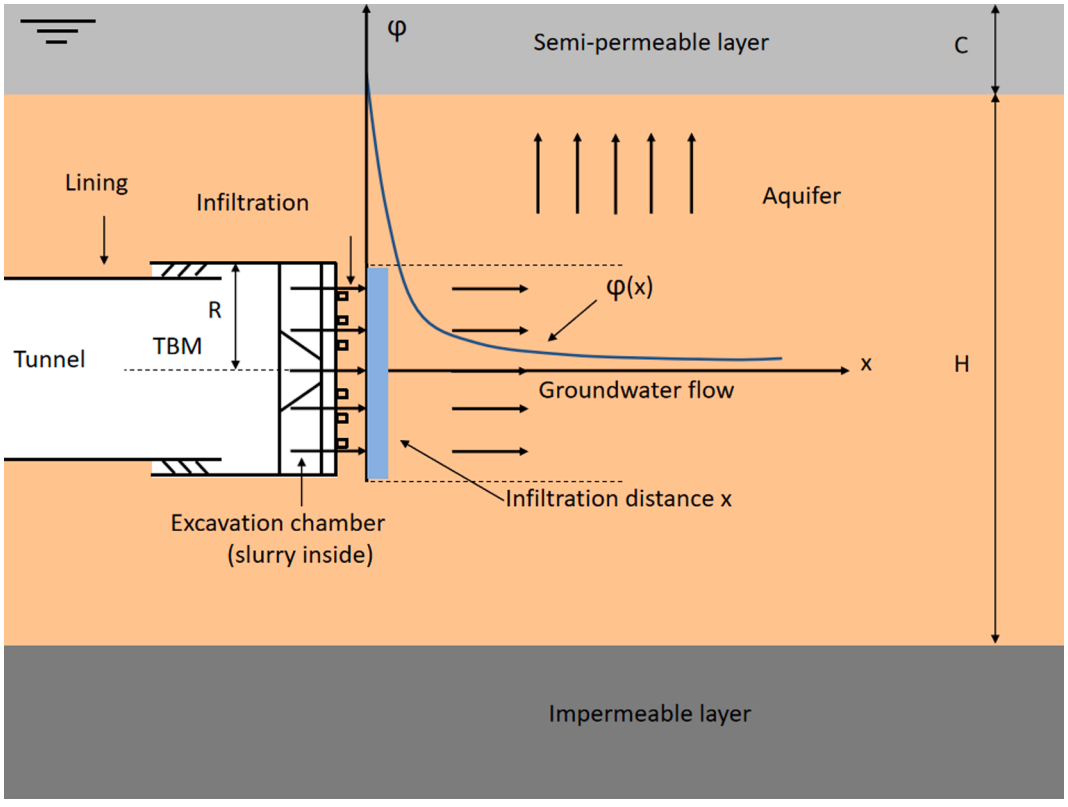

Fig. 1. A sketch of infiltration and groundwater flow generated by TBM tunnelling in a semi-confined aquifer.

of piezometric head at that location $\Delta\varphi$, and to the storage coefficient of the aquifer S. The storage coefficient S is a product of the thickness of the aquifer H and the volume of water released from storage dV_w by a unit decline of piezometric head $d\varphi$ for a volume V. That is:

$$S = H(dV_w/d\varphi)/V \tag{1}$$

The prototype situation is slightly different, as slurry infiltration from the TBM only occurs within the diameter of the TBM face, rather than over the whole height of the aquifer. The simplification of cylindrical flow, therefore, assumes that over the height of the aquifer, the piezometric head is constant and the only piezometric head variation occurs in the horizontal plane (Bezuijen and Xu, 2018). It is assumed that the groundwater flow caused by tunnelling is a radial flow in the horizontal plane beyond the radius of the TBM, and hence the solution is valid. In Fig. 2, the resulting isohypses in a horizontal plane at the height of the tunnel are sketched, which shows that the assumption of cylindrical flow is only reasonable at some distance from the tunnel face. At the tunnel face, the piezometric head is more or less constant and there will be no cylindrical flow pattern. However, it is assumed that the influence of this simplification is limited with respect to the solution further away from the tunnel, as has been shown for flow in an unconfined aquifer (Zizka et al., 2017, 2018).

The differential equation for a transient two-dimensional flow due to elastic storage in a semi-confined aquifer is:

$$\nabla^2(\varphi) = \frac{\partial^2\varphi}{\partial x^2} + \frac{\partial^2\varphi}{\partial y^2} = \frac{\varphi}{\lambda^2} + \beta^2\frac{\partial\varphi}{\partial t} \tag{2}$$

∇^2 is the Laplace operator and

$$\lambda^2 = \frac{k_s HC}{k_s'}, \quad \beta^2 = \frac{S}{k_s H}$$

where φ is the increase of piezometric head, (x, y) are coordinates in the horizontal plane with respect to the centre (0, 0) of tunnel face, λ is the leakage length of the aquifer, t is the time, k_s the hydraulic conductivity of the aquifer, k_s' is the hydraulic conductivity of the confining layer, H is the height of the aquifer, C is the height of the confining layer and S is the storage coefficient of the aquifer defined as 'the product of the thickness of the aquifer and the relative volume of water released from storage by a unit decline of head' (Jacob, 1946).

Various analytical and numerical cylindrical symmetric solutions for this differential equation are given, but none take into account the desired boundary condition of constant head. Therefore, a numerical solution was developed for such boundary conditions, using an explicit Forward Time Central Space (FWCS) difference method.

The differential equation in cylindrical coordinates for the flow in a semi-confined aquifer is:

$$\frac{\partial^2\varphi}{\partial r^2} + \frac{1}{r}\frac{\partial\varphi}{\partial r} = \frac{\varphi}{\lambda^2} + \beta^2\frac{\partial\varphi}{\partial t} \tag{3}$$

where r is the distance from the centre of the tunnel face.

The boundary conditions for this situation are:

$$r = 0 \rightarrow \varphi(0, t) = \varphi_0$$

$$r = \infty \rightarrow \frac{\partial\varphi}{\partial t}(\infty, t) = 0$$

It is assumed that at $t = 0$ the piezometric head is constant (taken zero in the paper) everywhere (for all r) and then the piezometric head at $r = 0$ is raised to φ_0. With this the model simulate that the filter cake (or infiltrated zone) is destroyed at $t = 0$ when excavation starts and then the soil comes in contact with the pressure in the mixing chamber. This may be incompletely right. In reality, the filter cake (or infiltrated zone) will be gradually destroyed and this process is not included in the analytical solution.

The initial condition is:

$$t = 0 \rightarrow \varphi(r, 0) = 0$$

The discretization of Eq. (3) is given by:

$$\varphi(r, t + \Delta t) = \varphi(r, t) + \frac{\Delta t}{\beta^2}\left[\frac{\varphi(r - \Delta r, t) - 2\varphi(r, t) + \varphi(r + \Delta r, t)}{(\Delta r)^2} + \frac{1}{2}\frac{\varphi(r + \Delta r, t) - \varphi(r - \Delta r, t)}{\Delta r \cdot r} - \frac{\varphi(r, t)}{\lambda^2}\right] \tag{4}$$

The remaining drawdown of piezometric head to time in a semi-confined aquifer in a cylindrical symmetric situation is the same as Eq. (4).

According to Bruggeman (1999), the steady state solution of Eq. (3) is:

$$\varphi(r) = \varphi_0\frac{K_0(r/\lambda)}{K_0(R/\lambda)} \tag{5}$$

where K_0 is the modified Bessel function of second kind, see Appendix B, and the approximation given in Eq. (5) is valid when $r/\lambda \ll 1$.

2.2. Coupled steady state model considering the influence of infiltration

Bezuijen et al. (2016) and Xu and Bezuijen (2018) showed that the excess pore water pressure around the TBM can be caused by slurry infiltration. In these models, a steady state flow is assumed. During standstill, slurry infiltration in the soil will continue until the maximum infiltration distance is reached. If the piezometric head far from the tunnel remains constant, the piezometric head in the sand just before the bentonite slurry front $\varphi(x)$, can be approximated as (Huisman, 1998):

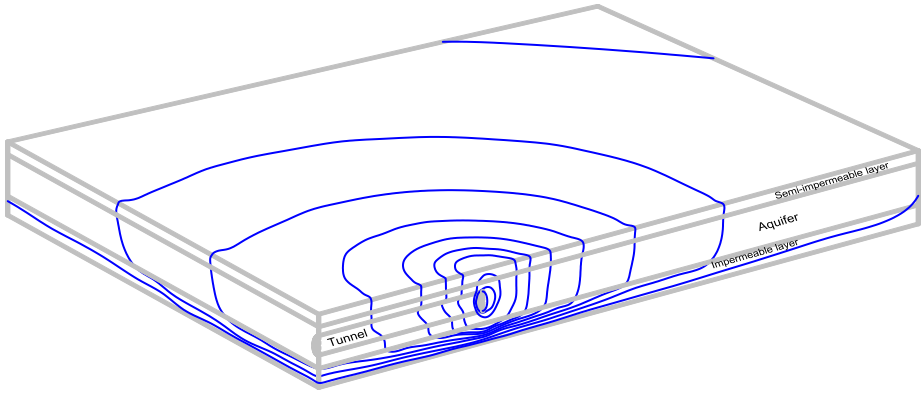

Fig. 2. Contour of excess pore water pressures generated by TBM tunnelling in a semi-confined aquifer. It is made on basis of the calculated result from a FEM modelling, in which a constant outflow boundary on the tunnel face is set and the undrained condition is applied to the whole model.

$$\varphi(x) = \varphi_{mx}\left(1 - \frac{x}{L}\right) - \frac{nv_p}{k_b}x \tag{6}$$

where φ_{mx} is the piezometric head in the excavation chamber, L the maximum infiltration distance, v_p the pore fluid velocity, k_b the hydraulic conductivity of sand for the bentonite slurry.

Eq. (6) assumes that there is no filter cake formation but only mud spurt during the slurry infiltration. This is true for the real TBM tunnelling in a sandy soil. In such a case, no 'clean' slurry but slurry containing sand will be present at the tunnel face. Xu and Bezuijen (2018) showed that, during infiltration of slurry containing sand, there will be no external filter cake but an internal low permeable layer formed. At the end of the slurry infiltration, infiltration distance x is equal to maximum infiltration distance L, and v_p and $\varphi(x)$ will tend to zero (Xu and Bezuijen, 2018).

In case of an unconfined aquifer, the flow in the sand just before the bentonite slurry front can be described, assuming radial flow, as (Bezuijen, 2002):

$$\varphi(x) = \frac{nv_p}{k_s}R \tag{7}$$

with R (m) the radius of tunnel. The value of φ_{mx} can be estimated from Eq. (6). Combing Eqs. (6) and (7), with $v_p = dx/dt$, it can be derived (Bezuijen et al. 2016):

$$\frac{dx}{dt} = \frac{\varphi_{mx}(1 - x/L)}{nR/k_s + nx/k_b} \tag{8}$$

with t the mud spurt time.

Integrating Eq. (7) with respect to t at $t = 0$ s, $x = 0$ m gives:

$$t = -\frac{nL}{\varphi_{mx}}\left[\left(\frac{R-L}{k_s} + \frac{L}{k_b}\right)\boldsymbol{ln}\left(\mathbf{1} - \frac{x}{L}\right) + x\left(\frac{\mathbf{1}}{k_b} - \frac{\mathbf{1}}{k_s}\right)\right] \tag{9}$$

Bezuijen and Xu (2018) have shown that Eq. (9) can also be used to approximate for the slurry infiltration in a semi-confined aquifer, when R is replaced by R_s, which takes the influence of the semi-confined aquifer on the flow into account:

$$R_s = \frac{\mathbf{1}}{\frac{\mathbf{1}}{R} - \frac{\mathbf{1}}{H} + \frac{\mathbf{1}}{H}\boldsymbol{K_0}\left(\frac{\mathbf{0.5}H}{\lambda}\right)} \tag{10}$$

From Eq. (8) the value of v_p can be determined, and hence Eq. (7) can be used to calculate the pore water pressure during excavation and during standstill. The pore water pressure during excavation can be similarly calculated, as presented by Xu and Bezuijen (2018).

3. Evaluations

A transient flow model for the excess pore water pressure generated by TBM tunnelling in a semi-confined aquifer and a quasi-static model coupled with the influence of slurry infiltration have been presented above. Here, the applicability of these models will be validated by comparing the calculated results with the measurements from the GHT that is constructed in a semi-confined aquifer, underneath the Noordplaspolder.

3.1. Results from the model considering the elastic storage of the aquifer

3.1.1. Parameters determination

The tunnel is bored through a saturated sand layer, where the overburden consists of peat and clay. The hydro-geotechnical conditions have been described in detail by Aime et al. (2004). The tunnel is constructed in a semi-confined aquifer where the Ring 2117, where the pore pressure transducers (PPTs) are installed (see Fig. 3), was located at the tunnel chainage 4219 m. The input parameters for the transient model are summarised in Table 1. The values of k_s, $\Delta\varphi$, H and C are obtained

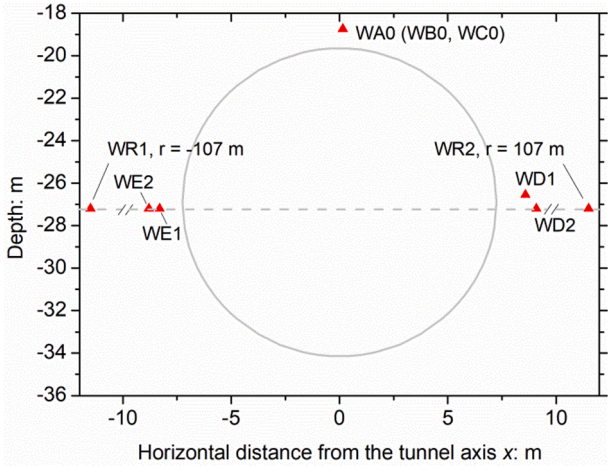

Fig. 3. The sketch of PPTs instrumented around ring 2117 at the GHT (after Xu and Bezuijen, 2018).

Table 1
Input values of parameters for the cylindrical solutions for the transient flow model.

$\Delta\varphi$ (m)	λ (m)	k_s (m/s)	k_s' (m/s)	H (m)	C (m)	S (–)	β^2 (m^{-2}·s)
2.2	205	1.5×10^{-4}	1×10^{-6}	35	8	5×10^{-4}	0.309

from measurements (Xu and Bezuijen, 2018). The head difference between the head, 8 m in front of the face, and the equilibrium head $\varphi_0 = 2.2$ m and TBM radius $R = 7.25$ m. The averaged hydraulic conductivity (k_s') of the overlying peat and clay layers was roughly set at 1.0×10^{-6} m/s, much smaller than the hydraulic conductivity (1.5×10^{-4} m/s) of the sand in the aquifer. Leakage length $\lambda = 205$ m, storability $S = 5 \times 10^{-4}$ and $\beta^2 = 0.309$ m^{-2}·s are calibrated by fitting the results from the transient cylindrical solution to the field measurement at $r = 8$ m. The distance indicates the distance between the TBM and ring 2117, where the PPTs WA0 and WR1 are located. Fig. 4 shows that the transient cylindrical solution well matches the measurement during excavation. During standstill, the pore pressure is slightly underestimated. The obtained parameters are then used for the predictions of excess pore water pressures at other distances.

From the steady state distribution of head, the value of transmitivity T (see Appendix B) can be determined using Theis' modified method (Jacob, 1946), assuming the leakage length λ is known. The storage coefficient S may be determined by Theis' method using the drawdown during the earliest phase of the transient state. Subsequently, the derived value of T can be checked.

The excess pore water pressures measured at GHT are compared with the steady state solution for the transient flow model (Eq. (4)) in Fig. 5. The excess pore water pressure far away from the tunnel was assumed to be zero, which corresponds with a pore water pressure of 153 kPa at the depth of the piezometer of WA0. As the measured pore water pressures are plotted as a function of distance, vertical downward spikes occur during TBM standstill as the excess pore pressures dissipate in time whilst the TBM is stationary. WR1 in the figure shows the results at place, 100 m perpendicular from the TBM. The model is a close match to the measurements close and far away from the tunnel.

3.1.2. Calculated results

The pore water pressures at distances of 16–28 m from the TBM, calculated from the transient analytical model (Eq. (4)), are plotted with the field measurements in time in Fig. 6. Fig. 6a, c and e show the increase of the pore water pressure after excavation starts, while Fig. 6b,

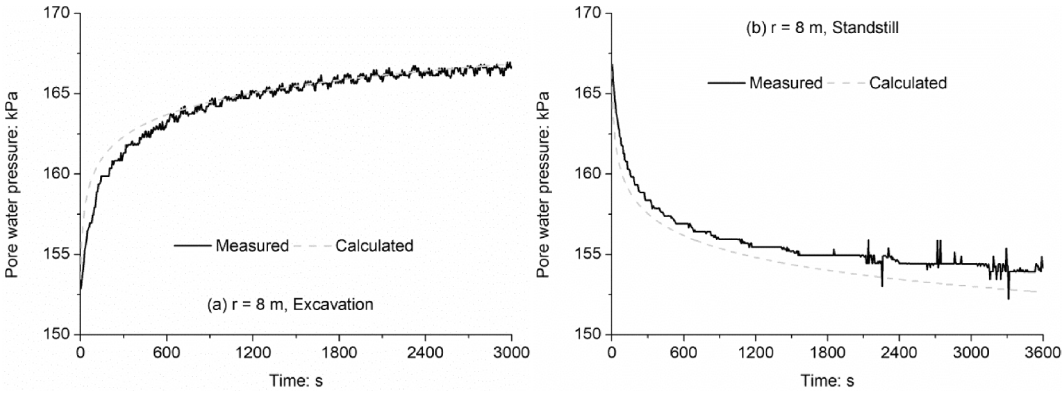

Fig. 4. Pore water pressures at $r = 8$ m, from the measurements and cylindrical flow model.

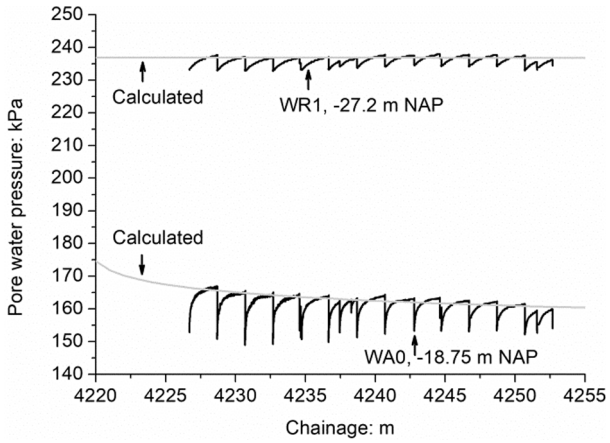

Fig. 5. Comparison of calculated and measured steady state pore water pressures at the GHT.

d and f show the delay during the standstill. The distances indicated in the figures are the distance between the TBM and ring 2117, where the PPTs WA0 and WR1 are located. TBM positions before ring 2117 are considered equivalent to positions after this ring (Kaalberg et al., 2014; Aime et al., 2004). It is shown that the transient model well agrees with the measurements during excavation at $r = 16$ m, but underestimates the pore water pressures at $r = 20$ and 28 m. It would be expected that the rate of rising and falling pore water pressures during excavation and standstill are the same for the same pressure difference. However, the TBM is continuously advancing during excavation, and at the location of the TBM the soil conditions can slowly change, and impact the measurements. For the distance $r = 107$ m that is far away from the TBM, as shown in Fig. 7, a similar effect is once again seen during standstill, and the cylindrical model predicts the measurements best from the start of the excavation phase. Clearer result can be observed from Figs. 8 and 9.

Figs. 8 and 9 show the relative transient pore water pressures at various distances from the TBM. It is clear that there is an effect of elastic storage. At the start of excavation/standstill, the pore water pressure further away from the TBM increases/decreases at a lower rate than closer by. On average the increase rate at $r = 8$ m is slightly faster than at $r = 28$ m, but the difference is limited.

From Figs. 8 and 9, it can be concluded that the measured lines are closer together than the calculated ones for $r = 8$ until $r = 28$ m. However, the calculated slower raise and fall of the pressure at $r = 107$ m is in good agreement with the measurements. Without elastic storage the lines should all on top of each other.

3.2. Results from the model coupling the effect of slurry infiltration

Figs. 10 and 11 show the results from the quasi-static cylindrical solution coupled with slurry infiltration (Eq. (7)) compared to the transient model (Eq. (4)) and measurements close to and far away from the tunnel face, respectively. It can be seen that the coupled model is in good agreement close to the tunnel face but underestimates the pore pressures away from the face. The maximum infiltration distance (L) has a significant influence on the results calculated with the coupled model. With increasing infiltration distance, the excess pore water pressure dissipates slower. This indicates that lower infiltration distance, and therefore controlling the bentonite quality, is important to ensure the stability of the tunnel face. Furthermore, as shown in Fig. 12, the leakage length λ influences the ratio between the excess pore pressures at 8 m and at 107 m. This is also the case in the transient solution.

4. Consequences for estimation of the stability of the tunnel face

Following van Rhee and Bezuijen (1992) and Broere (2015), Xu et al. (2020) argued that a minimum hydraulic gradient of 2 has to be maintained to achieve a vertical micro-stability of the tunnel face. For a semi-confined aquifer, assuming that there is spherical flow up to a distance equal to the thickness of the aquifer (H) and cylindrical flow beyond that point, the gradient at the tunnel face ($r = 0$) can be approximated from Eqs. (5) and (10) by integrating φ to r (Bezuijen and Xu, 2018):

$$i = \frac{\mathrm{d}\varphi}{\mathrm{d}r}\Big|_{r=0} = \frac{\varphi_0}{R}\frac{1}{1 - \frac{R}{H} + \frac{R}{H}K_0\left(\frac{0.5H}{\lambda}\right)} \tag{11}$$

where φ_0 is the piezometric head at the face; R the tunnel diameter, H the height of aquifer, x the distance from the centre of the tunnel face, λ the leakage length. K_0 is the modified Bessel function of second kind, see Appendix A.

For a 5 m radius tunnel in a 35 m high aquifer with leakage length of 205 m, a support pressure of 50 kPa (piezometric head of 5 m) a gradient $i < 2$ will be achieved at the face. This gradient is unable to achieve a stable body of cohesionless grains. This means that a stable face cannot be maintain when the tunnel are being drilling with water (a fact well known in practice). However, with a slurry with a 10 times lower permeability in the sand than the water, the gradient will be 10 times higher and normally stability is achieved. That's why tunnelling is done with slurry. For a 2.5 m diameter tunnel, the gradient will be larger than 2 and thus a stable tunnel face can be achieved.

In a limit analysis of the global stability of the tunnel face, to account for the presence of the excess pore water pressure, the distribution of excess pore water pressure in the soil mass surrounding the tunnel face should be used (Wang et al., 2013; Perazzelli et al., 2014; Huang et al., 2017). This can be obtained from a seepage analysis using FEM.

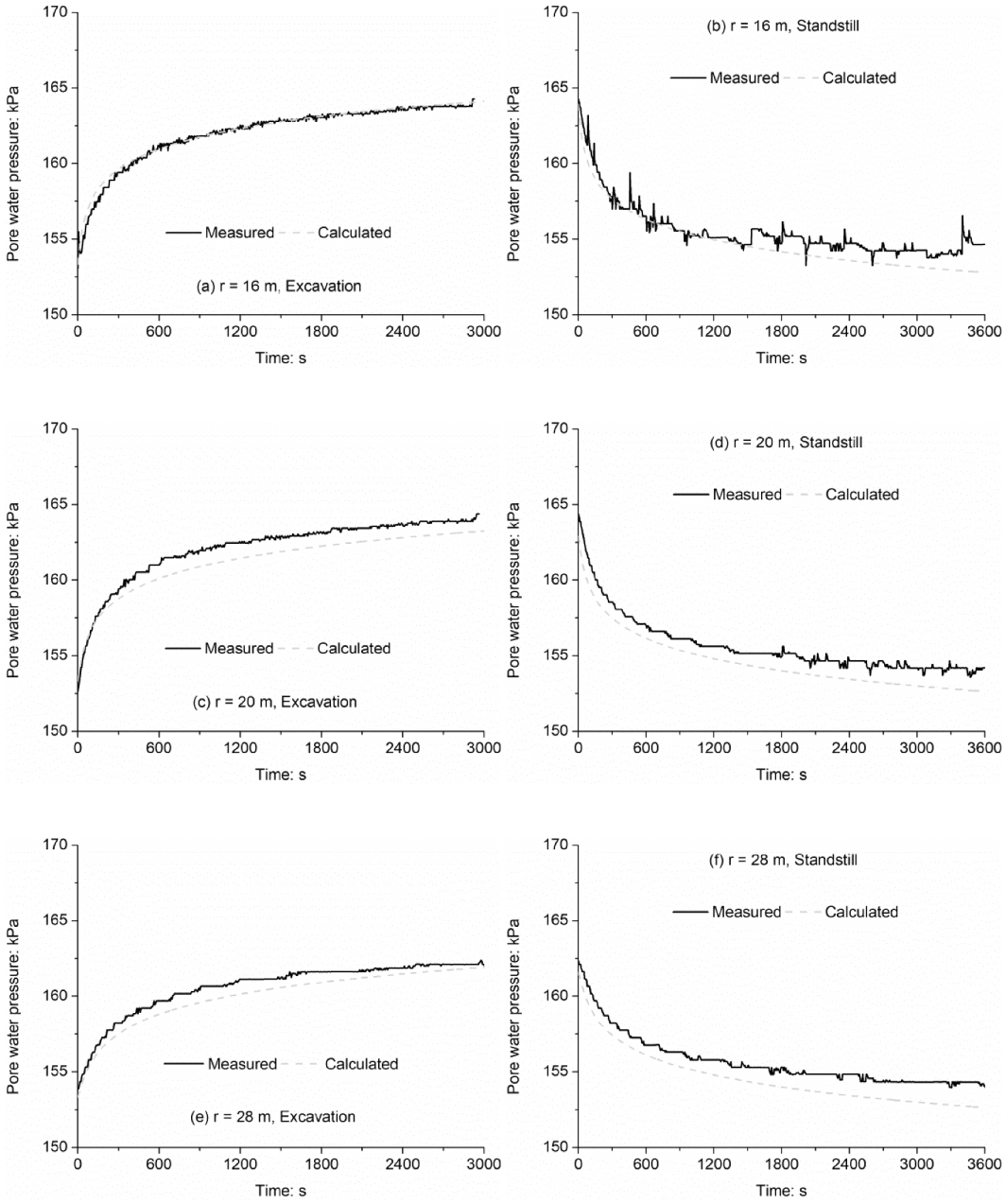

Fig. 6. Pore water pressures at various distances from the TBM, from the measurements and cylindrical flow model.

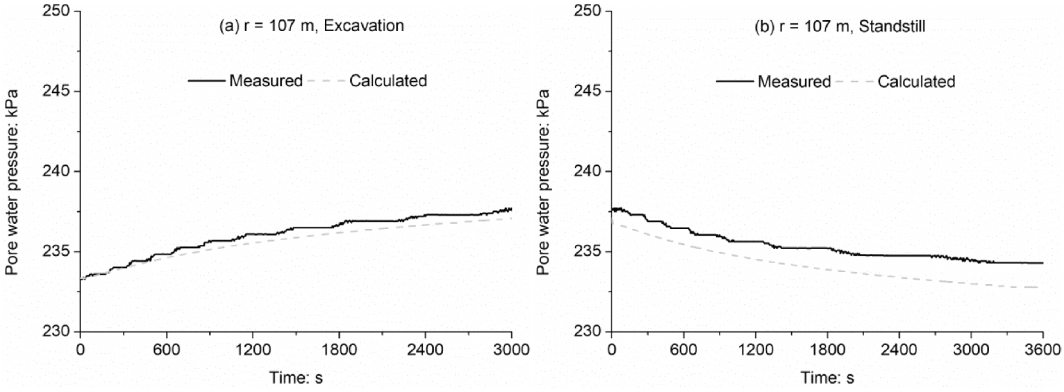

Fig. 7. Pore water pressures at various distances from the TBM, from the measurements and transient flow model.

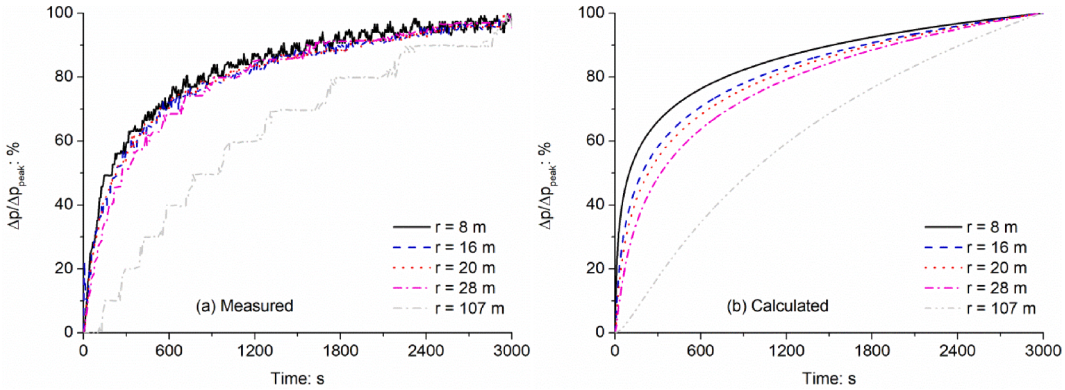

Fig. 8. Excess pore water pressures (a) measured at various distances from the TBM during excavation, and (b) calculated from the cylindrical flow model. $\Delta p/\Delta p_{peak}$: excess pore water pressure/the peak excess pore water pressure.

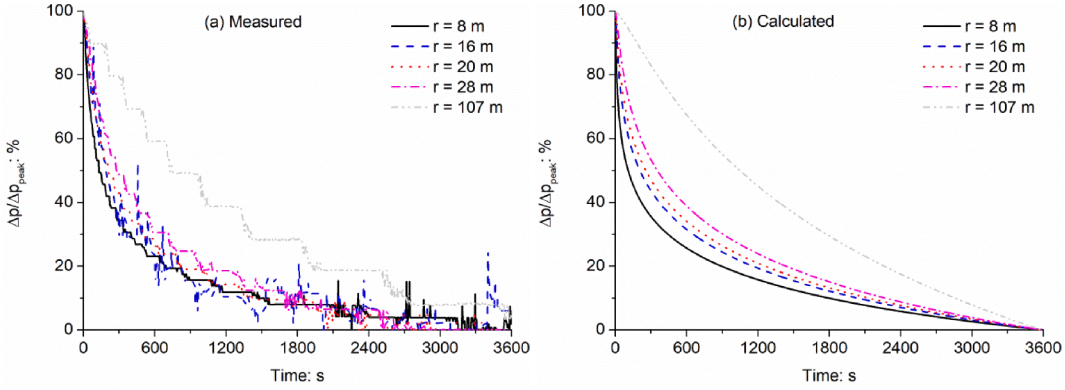

Fig. 9. Excess pore water pressures (a) measured at various distances from the TBM during standstill, and (b) calculated from the cylindrical model.

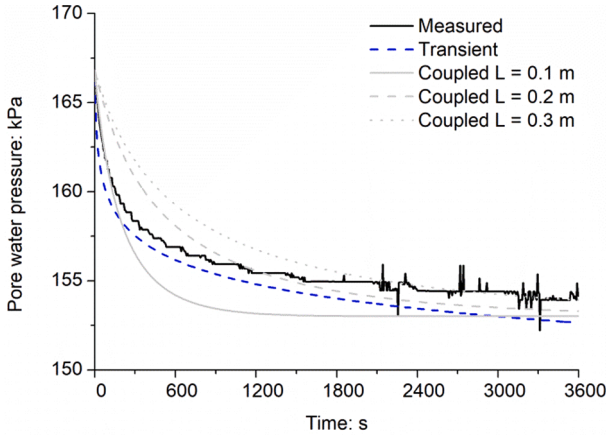

Fig. 10. The results calculated from the coupled model compared to other models and measurements during standstill close to the tunnel face. Leakage length $\lambda = 205$ m.

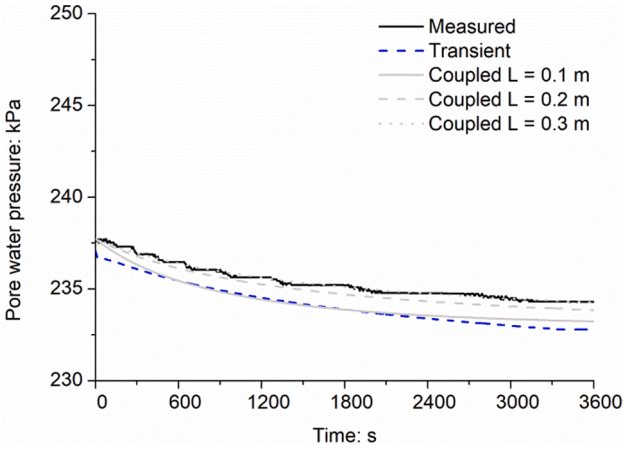

Fig. 11. The results calculated from the coupled model compared to other models and measurements during standstill far away from the tunnel face. Leakage length $\lambda = 205$ m.

However, the key factors that affect the stability of the tunnel face are difficult to directly identify. With a coupled calculation method, it is possible to calculate whether or not the front face is stable, as a function of the permeability of the slurry. Moreover, the effect of slurry infiltration is an extra complication. As an alternative, the models developed in this study provide an indication of the excess pore water pressure and reflect the effectiveness of the slurry infiltration. In this way, it is directly evident how factors such as the tunnel radius, thickness of the aquifer, leakage length of the aquifer and infiltration distance, affect the tunnel face stability.

5. Conclusions and recommendations

An analytical solution for the excess pore water pressures caused by TBM tunnelling in a semi-confined aquifer has been presented and an approach to couple the solution with the influence of slurry infiltration has been derived.

For the steady state, the model matches quite well with the measurements. This holds for measurements close to the TBM face, as well as far away from the TBM. This indicates that the excess pore pressures

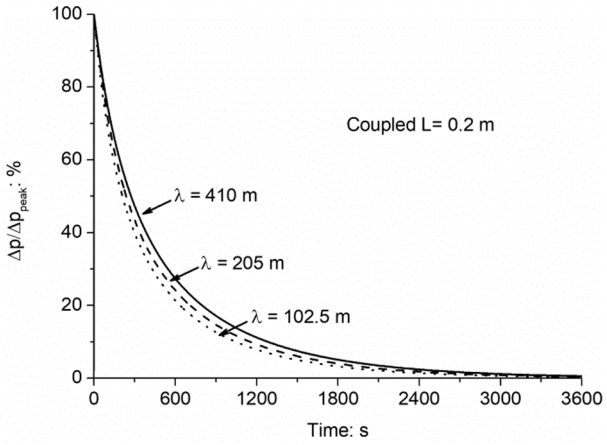

Fig. 12. The results calculated from the coupled model during standstill at $r =$ 8 m for various leakage lengths.

generated by TBM excavation are well matched by a cylindrical flow model in a semi-confined aquifer. For the transient state, the model also shows good agreement with the measurements.

The quasi-static cylindrical solution coupled with the influence of slurry infiltration shows good agreement with the measurements only for locations close to the tunnel face. Also, the maximum infiltration distance of the slurry, and therefore the slurry quality, has a significant influence on the calculation results. For a high permeable soil, a larger infiltration distance leads to a slower dissipation of excess pore water pressures. It does not make a difference during excavation (when excavation velocity is faster than the pore fluid velocity) and it gives a thicker impermeable layer when air pressure is necessary.

In a limit analysis of the stability of the tunnel face, the models developed are of interest to estimate the effects of the leakage length of the aquifer and infiltration distance.

Declaration of Competing Interest

The authors declare that they have no known competing financial interests or personal relationships that could have appeared to influence the work reported in this paper.

Acknowledgement

The first author would like to acknowledge the scholarship funded by China Scholarship Council and the Mobility Fund of Ghent University.

Appendix A

For a non-leaky confined aquifer, the differential function of the draw down at any time (t) is:

$$\frac{\partial^2\varphi}{\partial r^2}+\frac{1}{r}\frac{\partial\varphi}{\partial r}=\beta^2\frac{\partial\varphi}{\partial t} \tag{A1}$$

with $\beta^2 = \frac{S}{k_s D}$

The solution to Eq. (A1) is given by:

$$\varphi(r,t)=\frac{Q_0}{4\pi T}\int_{\frac{r^2 S}{4\pi T t}}^{\infty}\frac{e^{-u}}{u}\mathrm{d}u \tag{A2}$$

with $T = k_s D$

The remaining draw down at any instant in time after discharge at $x = 0$ has stopped is:

$$\varphi'(r,t')=\frac{Q_0}{4\pi T}\left(\int_{\frac{r^2 S}{4\pi T t}}^{\infty}\frac{e^{-u}}{u}\mathrm{d}u-\int_{\frac{r^2 S}{4\pi T t'}}^{\infty}\frac{e^{-u}}{u}\mathrm{d}u\right) \tag{A3}$$

Appendix B

$$K_0(x)=-\left\{ln\left(\frac{1}{2}x\right)+\gamma\right\}I_0(x)+\sum_{m=1}^{\infty}\frac{\left(\frac{1}{2}x\right)^{2m}}{(m!)^2(1+\frac{1}{2}+\frac{1}{3}+\cdots+\frac{1}{m})} \tag{B1}$$

$$I_0(x)=\sum_{m=0}^{\infty}\frac{\left(\frac{1}{2}x\right)^{2m}}{m!\Gamma(m+1)}=\sum_{m=0}^{\infty}\frac{\left(\frac{1}{2}x\right)^{2m}}{(m!)^2} \tag{B2}$$

$$\Gamma(m)=(m-1)!\ (m=1,\ 2,\ 3,\ \ldots) \tag{B3}$$

References

Aime, R., Aristaghes, P., Autuori, P., Minec, S., 2004. 15 m diameter tunneling under Netherlands polders. In: ITA Proceedings of Underground Space for Sustainable Urban Development, Singapore, Elsevier.

Autuori, P., Minec, S., 2005. Large diameter tunnelling under polders, Proceedings 5th Int. Symposium on Underground Construction in soft Ground, IS-Amsterdam 2005, Bakker, Bezuijen, Broere and Kwast (Eds.), Taylor and Francis Group, London, pp 181-186.

Bezuijen, A., 2002. The influence of soil permeability on the properties of a foam mixture in a TBM. Tunnelling. In: Proceedings of the 6th International Symposium of Geotechnical Aspects of Underground Construction in Soft Ground, IS-Lyon, Kastner, Emeriault, Dias, Guilloux (Eds), Taylor and and Francis Group, London, pp. 221–226.

Bezuijen, A., Pruiksma, J. P., van Meerten, H. H., 2001. Pore pressures in front of tunnel, measurements, calculations and consequences for stability of tunnel face. Proceedings of International Symposium on Modern Tunnelling Science and Technology, Tokyo.

Bezuijen, A., Steeneken, S.P., Ruigrok, J.A.T., 2016. Monitoring and Analysing Pressures Around a TBM. In: The 13th International Conference Underground Construction, Prague.

Bezuijen, A., Xu, T., 2018. Excess pore water pressures in front of a tunnel face when drilling in a semiconfined aquifer. ITA-AITES World Tunnel Congress, Dubai, pp. 2–10.

Bohlke, M., Rosenbaum, A., Boucher, D., 1996. Complex soil conditions and artesian groundwater pressures dictate different tunnelling methods and liner systems for Sections F6a, F6b and F6c of the Washington D. C. Metro. In: Proceedings, North American Tunnellling '96. Oydemir (Eds), Rotterdam, Netherlands: A. A. Balkema Publishers.

Broere, W., 2001. Tunnel Face Stability and New CPT Applications. PhD thesis. Delft University of Technology, Delft.

Broere, W., 2002. Influence of excess pore pressures on the stability of the tunnel face. In: Geotechnical Aspects of Underground Construction in Soft Ground, Kastner, Emeriault, Dias, Guilloux (Eds.) Toulouse, France, Taylor and Francis Group, London, pp. 179–184.

Broere, W., 2003. Influence of excess pore pressures on the stability of the tunnel face. Reclaiming the Underground Space ITA, Amsterdam, pp. 759–765.

Broere, W., 2015. On the face support of microtunnelling TBMs. Tunnelling Underground Space Technol. 46, 12–17.

Bruggeman, G.A., 1999. Analytical Solutions in Geohydrological Problems. Elsevier.

Cording, E., 2018. Monitoring and Controlling Ground Behavior at the Source Recent Applications to pressurized tunnelling. ITA-AITES World Tunnel Congress 2018, Dubai, United Arab Emirates.

Hamza, M., Ata, A., Roussin, A., 1999. Ground movements due to the construction of cut-and-cover structures and slurry shield tunnel of the Cairo Metro. Tunn. Undergr. Space Technol. 14 (3), 281–289.

Hoefsloot, F.J.M., 2001. Waterspanningen voor het boor[1]front: een eenvoudig geohydrologisch model. Geotechciek oktober. pp. 26–33. (in German).

Huisman, M., 1998. Static plastering, Theory and experiments, BTL – report 34, WL | Delft Hydraulics J1384. (In Dutch).

Huang, F., Pan, Q.J., Ling, T.H., 2017. Upper bound analysis of factor of safety for shield tunnel face subjected to underground water seepage. Chin. J. Geotech. Eng. 39 (8), 1462–1469.

Jacob, C.E., 1946. Radial flow in a leaky artesian aquifer. Trans. Amer. Geophys. Union 27 (2), 198–205.

Kaalberg, F.J., Ruigrok, J.A.T., De Nijs, R., 2014. TBM face stability and excess pore presssures in close proximity of piled bridge foundations controlled with 3D FEM. Proceeding of 8th International Symposium on Geotechnical Aspects of Underground Construction in Soft Ground.

Min, F., Zhu, W., Lin, C., Guo, X., 2015. Opening the excavation chamber of the large-diameter size slurry shield: A case study in Nanjing Yangtze River Tunnel in China. Tunn. Undergr. Space Technol. 46, 18–27.

Perazzelli, P., Leone, T., Anagnostou, G., 2014. Tunnel face stability under seepage flow conditions. Tunn. Undergr. Space Technol. 43, 459–469.

van Rhee, C., Bezuijen, A., 1992. Influence of seepage on stability of sandy slope. J. Geotech. Eng. 8, 1236–1240.

Wang, H.R., Huang, M.S., Lü, X.L., Zhou, W.Y., 2013. Upper-bound limit analysis of stability of shield tunnel face considering seepage. Chin. J. Geotech. Eng. 35 (9), 1697–1704.

Wu, H.N., Shen, S.L., Chen, R.P., Zhou, A., 2020a. Three-dimensional numerical modelling on localised leakage in segmental lining of shield tunnels. Comput. Geotech. 122, 103549. https://doi.org/10.1016/j.compgeo.2020.103549.

Wu, Y.-X., Shen, S.-L., Lyu, H.-M., Zhou, A., 2020b. Analyses of leakage effect of waterproof curtain during excavation dewatering. J. Hydrol. 583, 124582. https://doi.org/10.1016/j.jhydrol.2020.124582.

Xu, T., Bezuijen, A., 2018. Analytical methods in predicting excess pore water pressure in front of slurry shield in saturated sandy ground. Tunn. Undergr. Space Technol. 73, 203–211.

Xu, T., Zhou, W. H., Bezuijen, A., 2021. Modelling ground response to TBM tunnelling with active face support. Proceedings of the ISSMGE TC204-Symposium, 2020, Cambridge, UK (eds Mohammed Z.E.B. Elshafie, Giulia M.B. Viggiani, Robert J. Mair). London, UK: CRC Press.

Zheng, Y.F., Ding, Z.C., Dai, S.M., 2006. An analysis on surrounding ground deformation and gound/water pressure fluctuations caused by a super large diameter TBM. Chin. J. Undergr. Space Eng. 2 (8), 1349–1354.

Zizka, Z., Schoesser, B., Popovic, I., Thewes, M., 2017. Excess Pore Pressures in Front of the Tunnel Face During Slurry Shield Excavations due to Different Time Scales for Excavation Sequence of Cutting Tools and Penetration Time of Support Fluid. EURO: TUN 2017, Innsbruck University, Austria.

Zizka, Z., Schoesser, B., Thewes, M., Schanz, T., 2018. Slurry shield tunneling: New methodology for prediction of increased pore pressures resulting from slurry infiltration at the tunnel face under cyclic excavation processes. Int. J. Civil Eng. 4, 38. https://doi.org/10.1007/s40999-018-0303-2.

Wang, Z.-F., Shen, S.-L., Modoni, G., Zhou, A., 2020. Excess pore water pressure caused by the installation of jet grouting columns in clay. Comput. Geotech. 125, 103667. https://doi.org/10.1016/j.compgeo.2020.103667.